MODELING AFM TIP DYNAMICS THROUGH DIFFUSION IN TIME-PERIODIC POTENTIALS

JAMES PHILLIPS and KLAUS SCHULTEN
Department of Physics and Beckman Institute
University of Illinois at Urbana–Champaign
Urbana, IL 61801
USA

ABSTRACT. We consider the case of a chemically active AFM tip experiencing a bistable potential near a substrate while being driven by a periodic force of frequency Ω. The average position of such a tip traces a hysteretic loop which encircles an area $\pi\mathcal{H}(\Omega)$, which can reveal information on the tip-substrate interaction and on tip friction. We model this situation via a Smoluchowski diffusion equation and provide numerical results as well as construct asymptotic expansions for $\mathcal{H}(\Omega)$ in the limits of high and low frequency.

1 Introduction

Historically, the atomic force microscope (AFM) has been used in two modes: imaging and non-imaging [1, 2]. In the imaging mode the tip is scanned across the surface of the sample while a feedback circuit keeps the interaction with the surface constant. In the non-imaging mode the tip is slowly lowered to the surface and then retracted, allowing the elasticity of the sample and the adhesion force binding the tip to the sample to be measured. Recent applications of the AFM to biological systems have extended this method by fixing ligands to the tip, allowing the measurement of biologically significant interactions [3, 4, 5].

We consider in this contribution an extension of the non-imaging mode of op-

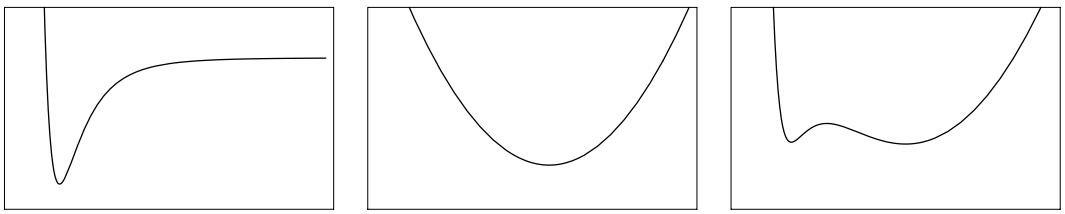

Figure 1: Example of the formation of a bistable potential between a substrate and the tip of an atomic force microscope. Left: Tip-substrate potential. Center: Harmonic potential due to AFM cantilever. Right: Bistable potential $V(x)$ comprising the sum of the tip-substrate and the cantilever potentials.

eration in which a chemically active AFM tip experiences a bistable potential due to an attractive tip-substrate potential and a quadratic potential accounting for a stiff cantilever. Figure 1 illustrates such a bistable potential. A bistable potential will only arise for certain tip positions and cantilever spring-constants, but once a suitable combination is found, information about the dynamics of the tip-substrate interaction can be readily abstracted, as demonstrated below.

In order to obtain such information we follow the suggestion in the lecture of Israelachvilli at this conference and assume that a weak periodic force of varying frequency be applied to the AFM tip. Such force could be supplied, for example, by magnetic material on the tip interacting with an external magnetic field or by the same mechanism which raises and lowers the tip. The periodic force causes the tip to repeatedly jump on and off the surface, tracing a hysteresis loop. Observation of this loop and its dependence on the frequency of the periodic force provides a view of the dynamics of the tip-substrate interaction, while regular adhesion experiments only explore the form of the tip-substrate potential.

The motion of the tip in the bistable tip-substrate potential with added periodic force can be characterized succinctly through the area enclosed by the hysteresis loop of the average tip position $\langle x(t) \rangle$. This area can be easily measured, requiring knowledge only of the relative deflection of the tip and of the phase of the sinusoidal driving force. Since this area corresponds to the work done by the driving force, alternative approaches to its measurement are available as well. We hope that our theoretical description of the hysteretic behavior of the AFM tip motion will motivate respective observations and serve for their analysis.

In this contribution we study hysteresis in a periodically driven stochastic system in the strong friction limit, both in general and in a symmetric bistable potential of the form $\frac{1}{4}x^4 - \frac{1}{2}x^2$ assuming a linear driving potential. Periodically driven stochastic processes have been the topic of recent study [6, 7], particularly with regard to the phenomenon of stochastic resonance. Perturbative approaches have been tried in the limits of small driving strength [8, 9]. Hysteresis in this type of system has been considered primarily in the deterministic limit [10] with some interest in the effects of thermal fluctuations [11, 12]. We consider hysteresis at all noise levels and driving strengths, in the high and low frequency limits.

In Section 2 we introduce the relevant stochastic description, define hysteresis, and comment briefly on numerical solutions. In Section 3 we present approximations for the hysteresis in the high and low frequency limits and a further approximation which holds in the limit of both low frequency and low temperature. In Section 4 we discuss our results.

2 Statement of Problem

Tip-sample adhesion experiments conducted on inorganic samples generally produce consistent and repeatable pull-off forces, while experiments on biological systems

produce a wide distribution of pull-off forces [4, 5]. One possible interpretation of these results is that thermal excitation of the tip plays a strong role in biological systems. In order to model the motion of a thermally excited tip we employ the Langevin equation

$$m\ddot{X} \;=\; -\,\partial_X U(X) \;-\; \gamma\dot{X} \;+\; \sigma\,\xi(t)\;. \tag{1}$$

Here the position of the tip is described by a coordinate X. The potential $U(X)$ represents the tip-substrate interaction. γ is the friction coefficient, σ is the rms value of the fluctuating force, and $\xi(t)$ represents white noise of unit strength characterized through

$$\langle\xi(t)\rangle \;=\; 0 \qquad \langle\xi(t)\xi(t')\rangle \;=\; \delta(t-t')\;. \tag{2}$$

γ and σ are related through the the fluctuation-dissipation theorem; it holds $\sigma^2 = 2k_BT\gamma$. For an effective mass of the tip on the order of nanograms, operation of the AFM in a physiological solvent and for frequencies of kHz or less the strong friction limit can be applied, i.e., the velocities of the tip can be assumed to obey the Maxwell distribution. In this limit the inertia term $m\ddot{X}$ can be neglected in (1) and the tip is governed by the stochastic differential equation [13, 14]

$$\dot{X} \;=\; -\,D\,\partial_X\beta U(X) \;+\; \sqrt{2D}\,\xi(t)\;. \tag{3}$$

where $\beta = 1/k_BT$ and $D = \sigma^2/2\gamma^2 = k_BT/\gamma$. Since one is interested in the average behavior of the tip position one prefers a description in terms of the probability $P(X,t)$ to observe the tip at position X at time t. Such a description is provided by the so-called Smoluchowski equation.

We will state in this section the Smoluchowski equation which we attempt to solve, extract the key parameters characterizing the system in this formulation, and define the quantity *hysteresis* which we use to account for the behavior of the system. We also comment briefly on the numerical solution of the Smoluchowski equation.

2.1 SMOLUCHOWSKI EQUATION

The probability distribution $P(X,t)$ for the tip position X corresponding to Eq. (3) is governed by the Smoluchowski equation [15]

$$\partial_t P(X,t) \;=\; \partial_X D\,(\partial_X + \beta\,U_X)\,P(X,t)\;. \tag{4}$$

The potential experienced by the tip, entering this equation, is of the form

$$U(X,t) \;=\; V(X) \;+\; W(X)\sin(\Omega t) \tag{5}$$

where $V(X)$ describes the bistable potential illustrated in Fig. 1. One can assume that $V(X)$ diverges for $X \to \pm\infty$ faster than W, ensuring that the location of the particle is bounded.

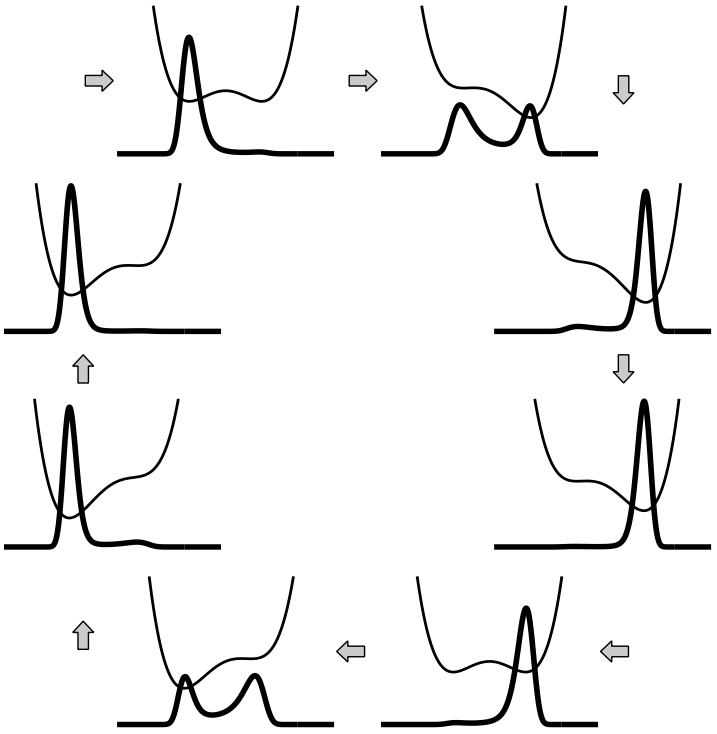

Figure 2: Hysteretic behavior of the distribution over a full cycle of the applied periodic force. Thin line: Potential $u(x,\theta)$. Thick line: "Steady-state" (see text) probability distribution $p(x,\theta)$ for $\omega = 0.1$, $\tau = 0.1$ ($\beta = 10$). The plot in the upper left corner corresponds to $\theta = 0$.

2.2 KEY PARAMETERS

In order to identify the key system parameters we introduce the dimensionless quantities $x = X/X_0$, $u = U/U_0$, $v = V/U_0$, $w = W/U_0$, $\theta = \Omega t$, $p = X_0 P$, and $\tau = k_B T/U_0 = 1/\beta$. Then (5) and (4) become

$$u(x,\theta) \;=\; v(x) \;+\; w(x)\sin(\theta) \tag{6}$$

$$X_0^2 \Omega\gamma\, \partial_\theta p(x,\theta) \;=\; \partial_x(U_0\tau\, \partial_x \;+\; U_0\, u_x)p(x,\theta)\;. \tag{7}$$

Defining $\omega = X_0^2\Omega\gamma/U_0$ allows one to write (7)

$$\omega\partial_\theta p(x,\theta) \;=\; \partial_x(\tau\partial_x \;+\; u_x)p(x,\theta)\;. \tag{8}$$

This identifies, besides $v(x)$ and $w(x)$, the two parameters ω and τ as the key characteristics of the system. These parameters describe the two basic properties of the tip dynamics: frequency and temperature; ω contains information on the frequency of the driving force relative to the relaxation time of the system and τ contains information on the temperature of the system relative to the energy scale of the potential.

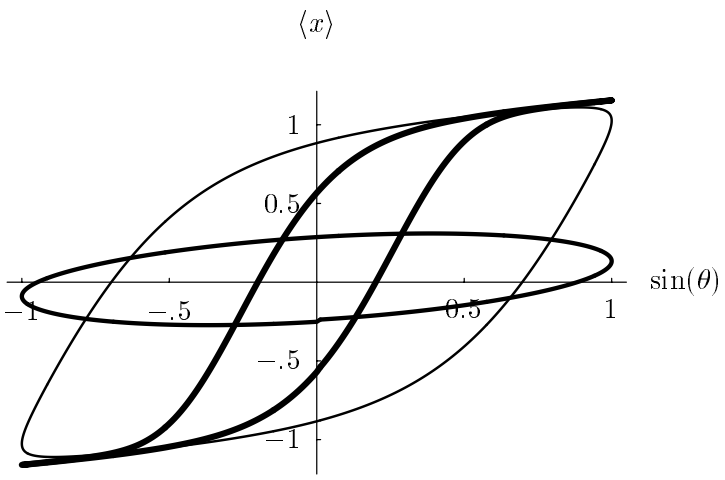

Figure 3: Hysteresis loops at high, moderate, and low frequencies. Note that time is in the counter-clockwise direction. Medium line: High frequency loop ($\omega = 1$, $\tau = 0.1$). Thin line: Moderate frequency loop ($\omega = 0.1$, $\tau = 0.1$). Thick line: Low frequency loop ($\omega = 0.01$, $\tau = 0.1$).

2.3 HYSTERESIS

We will explore only the "steady-state", or long-time behavior of the system, i.e., the behavior of the system after all of the transient modes have died out and $p(x, \theta)$ has become periodic in θ. This behavior is presented in Fig. 2. The figure compares the potential $u(x, \theta)$ with snapshots of the distribution $p(x, \theta)$ obtained through a numerical integration of (8). The snapshots are taken along the cycle of the periodic driving force. A plot of the average position $\langle x(\theta) \rangle = \int x\, p(x, \theta) dx$ as a function of $\sin(\theta)$ yields the hysteresis plots shown in Fig. 3. One obtains the corresponding distributions $p(x, \theta)$ as the Floquet eigenfunction with coefficient zero. We will use below that $p(x, \theta)$ can be expanded in a Fourier series, i.e.,

$$p(x, \theta) = a_0(x) + a_1(x) \cos(\theta) + b_1(x) \sin(\theta) + \cdots . \tag{9}$$

We wish to determine now the area $\mathcal{A}$ inside of the loop shown in Fig. 3, the so-called *hysteresis*, defined as

$$\mathcal{H} \equiv \frac{1}{\pi}\mathcal{A} = \frac{-1}{\pi} \oint \langle x(\theta) \rangle d \sin(\theta) \, . \tag{10}$$

Employing the Fourier expansion (9) one can express

$$\mathcal{H} = \frac{-1}{\pi} \int_0^{2\pi} \langle x(\theta) \rangle \cos(\theta) d\theta = - \langle a_1(x) \rangle . \tag{11}$$

Thus, the hysteresis is equivalent to the mean of the out-of-phase ($\cos(\theta)$) component of the Fourier expansion of $p(x, \theta)$. This result can be compared to the spectral power

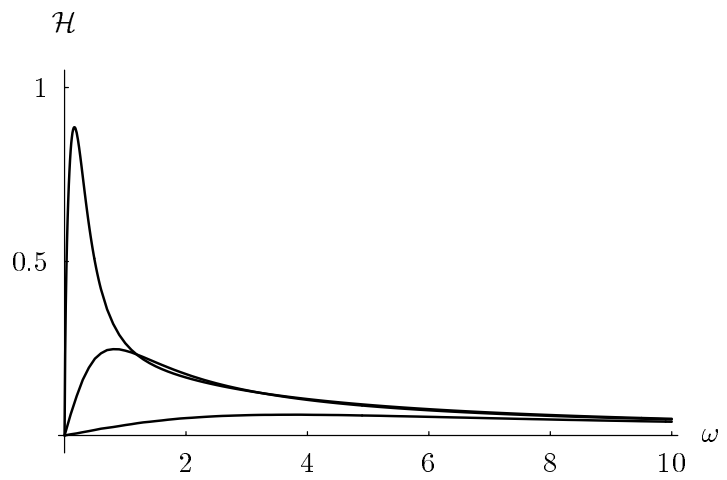

Figure 4: Hysteresis $\mathcal{H}$, as defined in (10), versus frequency ω for several temperatures. Top: Low temperature ($\tau = 0.1$). Middle: Moderate temperature ($\tau = 1$). Bottom: High temperature ($\tau = 10$).

amplification of interest in stochastic resonance, which is proportional to $\langle a_1(x)\rangle^2 + \langle b_1(x)\rangle^2$ [6].

Given a particular potential $u(x, \theta)$ we are interested in the ω– and τ–dependence of $\mathcal{H}$. We will determine $\mathcal{H}$ for the frequently-studied double-well potential of the form $v(x) = x^4/4 - x^2/2$ with a linear driving potential $w(x) = -\alpha x, \quad \alpha = 1/2$. Note that α has deliberately been chosen large enough to "dump" the distribution between the two wells twice each cycle, as shown in Fig. 2, and may therefore *not* be considered small.

The qualitative dependence of $\mathcal{H}$ on ω, presented in Fig. 4, may be deduced from the results shown in Fig. 3. At low frequencies, the tip position follows the changes in the potential almost adiabatically, with $\langle x(\theta)\rangle$ tracing out a narrow loop which extends to the locations of the two wells. But at sufficiently high frequencies the tip becomes too inert to respond to changes in the potential and $\langle x(\theta)\rangle$ remains nearly constant, actually tracing out a narrow, horizontal loop as shown in Figure 4. In both the high and low frequency limits, the hysteresis $\mathcal{H}$ becomes very small. Between these limits, $\mathcal{H}$ assumes large values for frequencies to which the tip can respond, albeit doing so "clumsily", showing a maximal perturbation by the periodic force applied. From Fig. 4 it can also be seen that lower temperatures generally result in a larger hysteresis. This is because at higher temperatures the barrier is more easily crossed by the distribution, allowing the system to respond to changes faster, and because the distributions are wider, favoring the middle of the potential.

2.4 NUMERICAL SOLUTIONS

The hysteresis behavior shown in Figs. 2, 3, 4 is based on a numerical solution of the Smoluchowski equation (4). Standard methods for the time-propagation of diffusion equations [16] were used for this purpose and (4) was integrated until the hysteresis did not change significantly between cycles. Then data were taken and the parameters were changed slightly. This reduced computation time by allowing relaxation of the system from an almost stable state for additional data-points.

3 Limiting Behavior

In this section we determine the hysteresis (10) in the limits of low and high frequency. This is done analytically through asymptotic expansions [17] in ω and $1/\omega$, respectively. The high frequency expansion obtained below, i.e., (14), is simple and independent of β, while the low frequency expansion derived below, i.e., (18), requires a numerical integration. For this reason we provide also a low temperature approximation (23) for the low frequency expansion, based on Kramers' approximation. Comparisons with numerical solutions are made for all cases.

In considering the experimental conditions to which this theory could be applied, we must consider which frequency ranges are relevant. The driving frequency cannot be so large that it is comparable to either the velocity relaxation rate or the resonant frequency of the tip. However, a high frequency reduces the amount of instrumental drift likely to be encountered. Conversely, a low driving frequency increases the amount of drift likely during a measurement. Also, at low temperatures the breakdown of our approximation with increasing frequency is extremely fast, reducing the applicability of the expansion. Moderate driving frequencies may contain more information, but its extraction is difficult since adequate analytical results are unavailable.

3.1 HIGH-FREQUENCY EXPANSION

In order to expand about the high-frequency limit we define $\varepsilon = 1/\omega$ and write (8)

$$\partial_\theta p(x,\theta) \;=\; \varepsilon\partial_x(\tau\partial_x \;+\; u_x)p(x,\theta). \tag{12}$$

In the high frequency limit holds $\varepsilon \;\ll\; 1$ and one may expand $p(x,\theta)$ as $p(x,\theta) = p_0(x,\theta) + \varepsilon p_1(x,\theta) + \varepsilon^2 p_2(x,\theta) + \cdots$. Substituting this expression into (12) yields

$$\partial_\theta[\,p_0(x,\theta)+\varepsilon p_1(x,\theta)+\varepsilon^2 p_2(x,\theta)+\cdots] \;=\; \varepsilon\partial_x(\tau\partial_x \;+\; u_x)[\,p_0(x,\theta)+\varepsilon p_1(x,\theta)+\cdots]\,. \tag{13}$$

Matching equal powers of ε generates a sequence of simpler equations for the functions $p_i(x,\theta)$. The first such equation, containing terms of order $O(\varepsilon^0)$, is $\partial_\theta p_0(x,\theta) = 0$. At high frequencies the sinusoidal driving force cancels itself out and only the time-averaged potential will influence the distribution. $p_0(x)$ thus characterized is given by

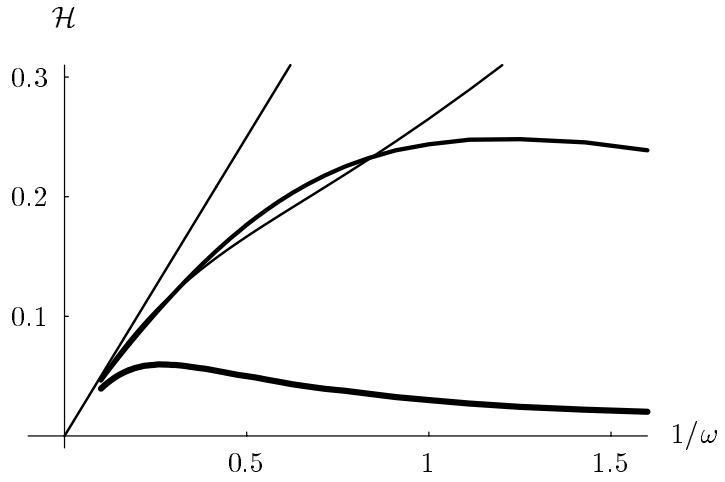

Figure 5: Hysteresis $\mathcal{H}$ versus $1/\omega$ illustrating the high-frequency expansion of the hysteresis. Straight line: Expression (14), i.e., $\mathcal{H} \sim \alpha/\omega = \frac{1}{2}/\omega$. Thin line: Low temperature ($\tau = 0.1$). Medium line: Moderate temperature ($\tau = 1$). Thick line: High temperature ($\tau = 10$).

the Boltzman distribution $p_0(x) = Ne^{-\beta\langle u\rangle_\theta} = Ne^{-\beta v(x)}$, where $N = \left(\int e^{-\beta v(x)}dx\right)^{-1}$ is a normalization constant.

The terms of order $O(\varepsilon)$ in (13) lead to the equation $\partial_\theta p_1 = N\sin(\theta)\partial_x(w_x e^{-\beta v(x)})$. This can be integrated to obtain $p_1 = -N\cos(\theta)\partial_x(w_x e^{-\beta v(x)})$. Comparison with (11) then gives, to order $O(\varepsilon)$,

$$\mathcal{H} = \varepsilon\int xN\partial_x(w_x e^{-\beta v(x)})dx = -\varepsilon\int Nw_x e^{-\beta v(x)}dx = \varepsilon\langle -w_x\rangle_{p_0} \tag{14}$$

where we have employed integration by parts and used $v(\pm\infty)\to\infty$. If the sinusoidal component of the potential is linear, i.e., for $w(x) = -\alpha x$, (14) can be expressed $\mathcal{H} = \alpha\varepsilon + O(\varepsilon^2)$. Thus, for a constant driving force holds $\mathcal{H}\sim\alpha/\omega$ where α is the amplitude of the driving force. Comparison with numerical results in Fig. 5 verifies this high frequency behavior.

3.2 LOW-FREQUENCY EXPANSION

We will now evaluate the hysteresis in the low frequency, or *adiabatic* limit, i.e., for $\omega \ll 1$. In the extreme case of this limit the system is time-reversible and follows the adiabatic Boltzman distribution $N(\theta)\exp[-\beta u(x,\theta)]$ where $N(\theta)$, in the present case, is a function of θ. We expand about this limit to determine the departure from it. For this purpose we substitute the expansion $p(x,\theta) = p_0(x,\theta) + \omega p_1(x,\theta) + \omega^2 p_2(x,\theta) + \cdots$, into (8) and obtain

$$\omega\,\partial_\theta[\,p_0(x,\theta)+\omega p_1(x,\theta)+\cdots\,] \;=\; \partial_x(\tau\partial_x + u_x)[\,p_0(x,\theta)+\omega p_1(x,\theta)+\omega^2 p_2(x,\theta)+\cdots\,]\,. \tag{15}$$

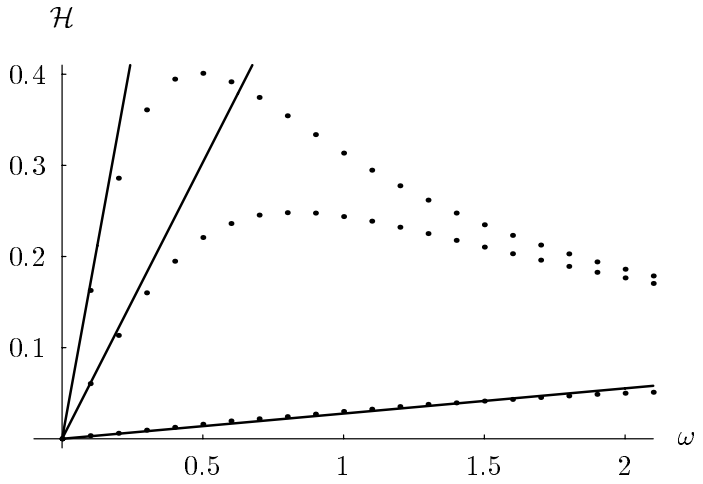

Figure 6: Hysteresis $\mathcal{H}$ versus ω illustrating the low-frequency expansion of the hysteresis. Straight lines: Expression (18) evaluated numerically. Top: Low temperature ($\tau = 0.5$). Middle: Moderate temperature ($\tau = 1$). Bottom: High temperature ($\tau = 10$).

Matching terms of order $O(\omega^0)$ results in $\partial_x(\tau\partial_x + u_x)p_0 = 0$, the solution of which is the Boltzman distribution. Matching terms of order $O(\omega)$ results in

$$\partial_\theta p_0(x,\theta) \;=\; \partial_x(\tau\partial_x \;+\; u_x)p_1(x,\theta) \tag{16}$$

which has a solution of the form $p_1(x,\theta) = M(\theta)p_0(x,\theta)+f(x,\theta)$ where f is a function yet to be specified. The condition $\int dx\, p_1 \;=\; 0$ implies for M the value $M = -\int f dx$.

In order to determine f, we rewrite (16) $\partial_\theta p_0 \;=\; \tau\partial_x e^{-\beta u}\partial_x e^{\beta u} f$ which can be solved by double quadrature. We choose the inner lower limit of integration as $-\infty$ to ensure convergence. Since the outer lower limit of integration corresponds to the addition of a constant multiple of $p_0(x,\theta)$, which will be adsorbed into $M(\theta)$ during normalization, we choose zero for convenience. Thus we arrive at

$$f(x) = \beta e^{-\beta u(x)} \int_0^x e^{\beta u(x')} \left[\int_{-\infty}^{x'} \partial_\theta p_0(x'')dx''\right] dx'. \tag{17}$$

This expression can then be evaluated numerically, for which purpose it is convenient to employ $\partial_\theta p_0 = \beta(\langle u_\theta\rangle_{p_0} - u_\theta)p_0$.

Normalizing the solution, as noted, and substituting into (11) gives, to order $O(\omega)$,

$$\mathcal{H} = \frac{-\omega}{\pi} \int_0^{2\pi} \left[\int_{-\infty}^{\infty} x \left(f(x,\theta) - p_0(x,\theta) \int_{-\infty}^{\infty} f(x',\theta)dx'\right) dx\right] \cos\theta d\theta. \tag{18}$$

Although cumbersome, this expression can be evaluated quickly by computer. Comparison with numerical simulations in Fig. 6 shows agreement. We also see that $\mathcal{H}$ increases quickly with β at small ω. Since $\mathcal{H}$ itself is bounded, the range of ω for which this linear approximation is valid, therefore, must also decrease.

3.3 LOW-TEMPERATURE BEHAVIOR OF LOW-FREQUENCY EXPANSION

In case of large β (small τ) one can simplify the low-frequency expansion (18). For this purpose we will employ Kramers' approximation [18] for the crossing rate of the potential barrier. This approximation is only valid in the limit of large barrier heights, measured in units of k_BT or, at present, in units of τ. In our model the barrier is reduced to zero during the cycle. However, since we are in the adiabatic limit the vast majority of the distribution will have crossed the barrier before the barrier becomes small and, therefore, the flux will be negligible when Kramers' approximation is invalid. Of course, when β is not large the barrier height is *never* large and so our approximation breaks down.

In our present approximation the potential $u(x,\theta)$ (6) will be characterized through the following quantities: the magnitudes of the second derivatives at the bottom of the left and right well, ω_A^2 and ω_B^2, respectively; the magnitude of the second derivative at the barrier maximum , $-\omega_C^2$; the height of the barrier going from left to right and right to left, u_A and u_B, respectively; the fraction of tips in the left and in the right well, N_A and N_B, respectively. The latter quantities obey, in the limit of high barriers, the rate equation

$$\dot{N}_A = -k_A N_A + k_B N_B \tag{19}$$

$$\dot{N}_B = -k_B N_B + k_A N_A \tag{20}$$

where, according to Kramers' approximation, holds $k_A = \frac{\omega_A\omega_C}{2\pi\gamma}e^{-\beta u_A}$ and $k_B = \frac{\omega_B\omega_C}{2\pi\gamma}e^{-\beta u_B}$.

In case of the bistable potential $v(x) = x^4/4 - x^2/2$ the wells remain approximately at ± 1 and the maximum at $x = 0$. Accordingly, we assume $\omega_A = \omega_B \approx \sqrt{2}$ and $\omega_C \approx 1$. Similarly we approximate $u_A \approx \frac{1}{4} - \alpha\sin(\theta)$ and $u_B \approx \frac{1}{4} + \alpha\sin(\theta)$. Note that u_A actually becomes negative but, as explained above, at this point holds $N_A \ll 1$ such that the terms $k_A N_A$ in (19, 20) are negligible. Recognizing that for $\beta \gg 1$ the tip will sit near the bottoms of the wells, one can assume $\langle x\rangle \approx N_B - N_A = 2N_B - 1 = 1 - 2N_A$. The rate equations (19, 20) yield then

$$\langle x\rangle_\theta \;=\; \frac{\sqrt{2}}{\pi\omega}e^{-\beta/4}\left[\sinh(\frac{\beta}{2}\sin(\theta)) - \langle x\rangle\cosh(\frac{\beta}{2}\sin(\theta))\right]. \tag{21}$$

Expression (21) is still too unwieldy for an evaluation of $\mathcal{H}$ according to (10). However, one can expand (21) in terms of the small parameter $\varepsilon = \omega e^{\beta/4}$. One eventually obtains

$$\langle x(\theta)\rangle \;\sim\; \tanh(\frac{\beta}{2}\sin(\theta)) + \varepsilon\left(\frac{-\beta\pi}{2\sqrt{2}}\cos(\theta)\mathrm{sech}^3(\frac{\beta}{2}\sin(\theta)) + \tanh(\frac{\beta}{2}\sin(\theta))\right). \tag{22}$$

In evaluating the integral (10) to obtain $\mathcal{H}$ one exploits $\beta \gg 1$ to obtain finally the simple expression

$$\mathcal{H} \sim \frac{\omega e^{\beta/4}\pi}{\sqrt{2}} \quad (\beta \gg 1,\ \omega \ll e^{-\beta/4}). \tag{23}$$

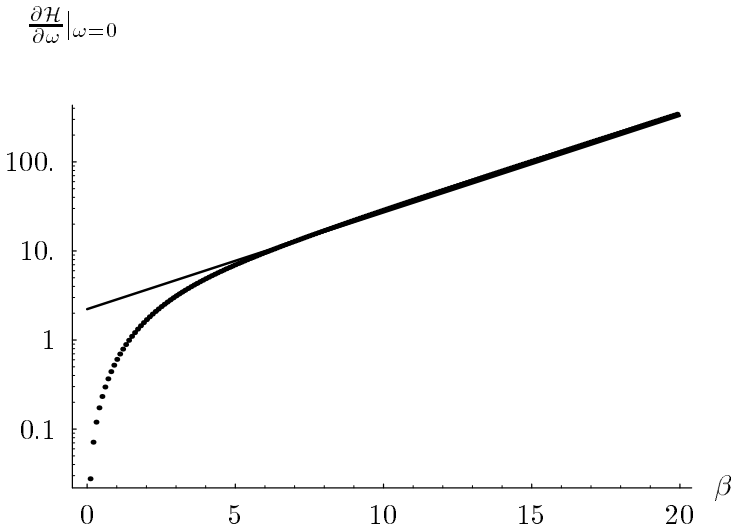

Figure 7: $\frac{\partial \mathcal{H}}{\partial \omega}|_{\omega=0}$ versus β showing low-temperature (large-β) agreement. Dotted line: Evaluation according to the low-frequency expansion. Straight, solid line: Evaluation according to (23).

As demonstrated in Fig. 7, this approximation is in excellent agreement with the numerically integrated low-frequency expansion; given the number of approximations involved in the derivation of (23) this is a surprising, but welcome result.

4 Discussion

In this contribution we have provided the theoretical framework for a description of an AFM tip subject to a bistable interaction with a substrate, moving in the strong friction limit (solvent), and being subject to a periodic driving force. This scenario should be applicable to AFM studies of biological systems using chemically active tips. The theoretical description is based on the Smoluchowski equation which describes diffusion in the presence of a force field.

The aim of this contribution is to show that the measurement of the hysteresis loop traced by the AFM tip, in particular, the measurement of the area circumscribed by this loop, the so-called hysteresis, can yield valuable insight into the microscopic interaction between tip and substrate, and into the dynamics of the tip, i.e., the tip's friction coefficient. In order to relate the hysteresis to microscopic properties one needs simple expressions which can be inverted to yield the mentioned quantities, once the hysteresis has been measured. For this purpose we have provided asymptotic expansions for the hysteresis in the limits of high (14) and low (18) frequency of sinusoidal forces. The expressions are valid for arbitrary temperatures and driving amplitudes. In addition, we have simplified the low-frequency expansion in the limit of low temperature (23) for the case of a simple bistable potential. The validity of the

expansions provided has been demonstrated via comparison with numerical results.

The simplicity of the high-frequency expansion (14) in the case of a linear driving potential is particularly striking and useful. The independence of the hysteresis of both temperature and form of the potential suggests that this limit may be useful for determining the friction coefficient γ in an experimental situation where Ω, α, and $\mathcal{H}$ are known.

The complexity of the low-frequency expansion (18) makes it difficult to invert. In addition, the large slope and limited validity range of this expansion reduce its applicability. However, this expansion may be useful in the study of hysteresis in the deterministic limit.

The range of situations that could be studied in AFM experiments is not limited to symmetric, double-well potentials as studied here. For actual experiments experimenters may prefer to operate in the range of large-hysteresis and moderate frequencies, i.e., in a range not covered by the approximations provided. These situations might well be approached using numerical solutions of the Smoluchowski equation. This possibility to obtain, from measured hysteresis values, information for arbitrary potentials and frequencies should not be discounted.

Acknowledgments

We thank Peter Jung for helpful comments and Manfred Radmacher for tutoring us on atomic force microscopy. J.P. thanks the Fannie and John Hertz Foundation and the University of Illinois for support. This work was supported by grants from the National Institutes of Health (PHS 5 P41 RR05969-04) and the Roy J. Carver Charitable Trust.

References

[1] G. Binnig, C. F. Quate, and Ch. Gerber. Atomic force microscope. *Physical Review Letters*, 56(9):930–933, 1986.

[2] D. Rugar and P. Hansma. Atomic force microscopy. *Physics Today*, October 1990.

[3] C. Bustamante, D. A. Erie, and D. Keller. Biochemical and structural applications of scanning force microscopy. *Current Opinion in Structural Biology*, 4:750–760, 1994.

[4] E.-L. Florin, V. T. Moy, and H. E. Gaub. Adhesion forces between individual ligand-receptor pairs. *Science*, 264:415–417, April 1994.

[5] V. T. Moy, E.-L. Florin, and H. E. Gaub. Intermolecular forces and energies between ligands and receptors. *Science*, 266:257–259, October 1994.

[6] P. Jung. Periodically driven stochastic systems. *Physics Reports*, 234(4 & 5):175–295, 1993.

[7] P. Jung. Thermal activation in bistable systems under external periodic forces. *Z. Phys. B.*, 76:521–535, 1989.

[8] C. Presilla, F. Marchesoni, and L. Gammaitoni. Periodically time-modulated bistable systems: Nonstationary statistical properties. *Physical Review A*, 40(4):2105–2113, 1989.

[9] L. Gammaitoni, E. Menichella-Saetta, S. Santucci, and F. Marchesoni amd C. Presilla. Periodically time-modulated bistable systems: Stochastic resonance. *Physical Review A*, 40(4):2105–2113, 1989.

[10] P. Jung, G. Gray, and R. Roy. Scaling law for dynamical hysteresis. *Physical Review Letters*, 65(15):1873–1876, 1990.

[11] M. C. Mahato and S. R. Shenoy. Hysteresis and stochastic resonance: A numerical study of a double-well potential. *Physical Review E*, 50(4):2503–2512, 1994.

[12] M. Rao. Comment on "Scaling law for dynamical hysteresis". *Physical Review Letters*, 68(9):1436, 1992.

[13] C. W. Gardiner. *Handbook of Stochastic Methods*. Springer, Berlin, 1983.

[14] N. G. van Kampen. *Stochastic Processes in Physics and Chemistry*. North-Holland, Amsterdam, 1981.

[15] H. Risken. *The Fokker-Planck Equation*. Springer, Berlin, 1984.

[16] W. H. Press, S. A. Teukolsky, W. T. Vetterling, and B. P. Flannery. *Numerical Recipies in C*. Cambridge, second edition, 1992.

[17] E. J. Hinch. *Perturbation Methods*. Cambridge, 1991.

[18] H. A. Kramers. *Physica (The Hague)*, 7:284, 1940.